Modeling and simulation of noise in transistors under large-signal condition

(Article begins on next page)

25 December 2024

Facile synthesis, structure and visible light photocatalytic activity of recyclable ZnFe2O4/TiO2

Xiaodi Zhua, Fan Zhanga, Mengjiao Wang b, Jianjun Dinga,b, Song Suna,b,∗, Jun Baoa,b, Chen Gaoa,b,∗

a National Synchrotron Radiation Laboratory, Collaborative Innovation Center of Chemistry for Energy Materials, University of Science & Technology of China, Hefei, Anhui 230029, China

b CAS Key Laboratory of Materials for Energy Conversion, Department of Materials Science and Engineering, University of Science & Technology of China, Hefei, Anhui 230026, China

Abstract: A kind of sponge-like ZnFe2O4/TiO2 composite was facilely synthesized by a solution combustion method. The physicochemical properties, including the crystalline phase, surface morphology, spectral response, photogenerated charge carriers' separation and transfer efficiency, were characterized by X-ray diffraction, scanning electron microscopy, transmission electron microscopy, N2 adsorption/desorption isotherms, X-ray photoelectron spectroscopy, UV–vis absorption spectroscopy and photoluminescence spectroscopy techniques and analyzed to interpret the relationship between the structure and photocatalytic activity. The sponge-like morphology promotes the adsorption of reaction species as well as functions as a good light harvesting structure for the enhancement of spectral utilization. The heterojunctioneffectively inhibitedthe recombination of photogenerated charge carriers. Withthese synergistic effects, the degradation rate of methylene blue on ZnFe2O4/TiO2 was up to 93.2% under visible light irradiation and remained stable even after five consecutive reaction runs. Moreover, owing to the magnetic property, ZnFe2O4/TiO2 can be recycled easily. Additionally, a photocatalytic mechanism of ZnFe2O4/TiO2 was proposed.

1. Introduction

Since the success of hydrogen production through electrochemical photolysis by Fujishima and Honda [1], extensive attempts have been made to design and synthesize potential photocatalysts in view of environmental remediation and renewable hydrogen by water splitting [2,3]. Among these photocatalysts, TiO2 has attractedmuch attention due to its nontoxicity, low cost, and chemical stability [4]. However, an inefficient utilization of solar energy originated from its large band gap energy (~3.2 eV) and fast recombination of photogenerated charges limits its practical applications seriously [5]. Therefore, many attempts aimed at improving the photocatalytic activity of TiO2 under visible light irradiation have been made, such as metal deposition [6,7], ion doping [8–12], dye sensitization [13,14],

and semiconductor coupling [15,16]. It was realized that the construction of interface structure to form heterojunction is considered as an effective tool to expand the spectral response and promote the separation of electrons and holes [17,18]. Particularly, zinc ferrite ($ZnFe_2O_4$) seems to be a potential candidate semiconductor available for coupling with TiO_2 and has aroused much interest owing to its specific electronic structure, which has been demonstrated in the application fields of electronic devices and magnetic resonance imaging [19,20]. On the one hand, $ZnFe_2O_4$ with a narrow bandgap of 1.9 eV could be an outstanding sensitizer for wide bandgap semiconductors [21]. On the other hand, the appropriate potential position of valence band (VB) and conduction band (CB) of $ZnFe_2O_4$ seems to be favorable to effectively separate the charge carriers when coupling it with TiO_2 [22]. Subsequently, the preparation methods and physicochemical properties of $ZnFe_2O_4/TiO_2$ composite have been widely investigated in order to enhance the photocatalytic activity. Yuan and Zhang [16] prepared $ZnFe_2O_4/TiO_2$ nanoparticles via a colloid chemical method and indicated that coupling $ZnFe_2O_4$ with TiO_2 could improve the photocatalytic activity compared withpure TiO_2. Wang and his co-workers [22] reported a hydrothermal deposition route to synthesize TiO_2 nanotube array modified with $ZnFe_2O_4$ nanoparticles, and attributed the high photocatalytic activity to the enhanced photogenerated electron–hole separation and the improved transfer efficiency of photogenerated charge carriers. Li et al. [23] confirmed this speculation by photoluminescence, surface photovoltage and transient photovoltage analysis. It indicated that the separation of the charge carriers could undergo the processes of ultra-fast injection from $ZnFe_2O_4$ to TiO_2 and then diffusion in the TiO_2 nanotubes. Hou et al.[24] observed the migration efficiency of photogenerated carriers at the $ZnFe_2O_4/TiO_2$ interface by photoelectrocatalytic test. It was found that the separation and migration of charge carriers at the $ZnFe_2O_4/TiO_2$ interface are directly affected by the heterojunction structure formed during the preparation process. In order to further refine the particular heterojunction structure, sol–gel method [25,26], coprecipitation hydrolysis method [27,28], hydrothermal method [29] and liquid/solid synthesis method [30,31] were developed in succession. However, in most cases, a large amount of organic salts, surfactants accompanied with the harsh conditions during synthesis process and the relatively low energy conversion to production still hindered the scale-up preparation and environmental protection. In this paper, a kind of sponge-like $ZnFe_2O_4/TiO_2$ composite was synthesized by a facile solution combustion (SC) method rapidly and environmental friendly. The $ZnFe_2O_4/TiO_2$ heterojunction exhibited high photocatalytic activity of degradating methylene blue (MB) under visible light irradiation. Additionally, the photocatalytic mechanism and the structure-to-activity relationship were proposed.

2. Experimental

2.1. Preparation of photocatalysts The anatase TiO_2 nanoparticles were synthesized through sol–gel method. The procedure was as follows: 32 ml ethanol (CH_3CH_2OH, CP) and 10 ml tetrabutyl titanate ($Ti(OC_4H_9)_4$, CP) were mixed and kept stirring for 15 min. Then 3.4 ml deionized water and 4.0 ml acetic acid (CH_3COOH, AR) mixture solution was added into the above solution dropwise and stirred constantly for 30 min. After aging at room temperature for 48–96 h, the gel was dried at 353K for 48 h. Finally, the sample was annealed at 753K for 5 h to form anatase TiO_2 nanoparticles. $ZnFe_2O_4/TiO_2$ samples were facilely prepared at a relatively low temperature by a solution combustion method. In a typical synthesis, 1.490 g zinc nitrate ($Zn(NO_3)_2·6H_2O$, AR), 4.040 g ferric nitrate ($Fe(NO_3)_3·9H_2O$, AR) and 1.950 g glycine (NH_2CH_2COOH, AR) were completely dissolved in 50 ml deionized water in a beaker under magnetic stirring. Then 0.160 g TiO_2 were added to the solution. After continuous vigorous stirring, the beaker was transferred to a temperature programmed tube furnace to proceed the reaction. In the first heating treatment, the mixed solution was heated to 423K in 30 min and kept for 10 min to evaporate the excess water. Then it was heated to 623K which is high enough to ignite the glycine for triggering the solution combustion reaction and kept for 60 min. As gases generated during the reaction, the fluffy and porous sponge-like $ZnFe_2O_4/TiO_2$ composite was formed. The pure $ZnFe_2O_4$ for the controlling experiments was prepared through the samemethod without adding TiO_2.Allthe reagents were purchased from Sinopharm Chemical Reagent Co., Ltd. and were used without further purification.

2.2. Characterization X-ray diffraction (XRD) was performed on a MacScience MXPAHF diffractometer with Cu K radiation (= 0.15418 nm) in the range of 2 = 10–80∘. Scanning electron microscopy (SEM) images were taken by using a field emission scanning electron microscope (JEOL JSM-6700F) with an accelerating voltage of 20 kV. High resolution transmission electron microscopy (HRTEM) analysis was performed on a transmission electron microscope (JEM-2011). A selected area energy dispersive X-ray spectrum (EDS) was obtained on the JEM-2011 TEM. Nitrogen adsorption–desorption isotherms were measured on a surface area and porosity analyzer (ASAP 2020) to further characterize the morphology of the samples. X-ray photoelectron spectroscopy (XPS, ESCALAB250) measurements were employed to analyze the chemical composition. All the binding energy was referenced to the adventitious C1s peak at 284.8 eV. UV–vis diffuse reflectance spectra (UV–vis DRS) were recorded by a UV–vis absorption spectrometer (Solidspec DUV-3700) and photoluminescence spectra (PL) were obtained by a fluorescence spectrophotometer (Fluroolog3-tau-p) with a xenon lamp as the excitation source at room temperature. An electron spin resonance (ESR) signal of the hydroxyl radicals spin trapped by 5,5-dimethyl-1-pyrroline-Noxide (DMPO) was recorded on a JES FA200 X-band spectrometer under irradiation with a 500W Xenon lamp. 2.3. Photocatalytic activity test Photocatalytic activity

was evaluated by decomposing MB in aqueous with the initial concentration of 20 mol L−1 on a homemade apparatus under visible light irradiation. A 300W halogen tungsten lamp was used as the radiation source. 0.100 g photocatalyst powders were dispersed into 150 ml MB solution in a quartz photoreactor. The reaction temperature was controlled at room temperature by circulating cooling water with a water jacket. Before irradiation, the suspensions were stirred for 30 min in darkness to ensure that the MB molecules could reach the adsorption/desorption equilibrium on the photocatalyst surface. At intervals, 3 ml solutionsuspension was withdrawnandcentrifuged. The filtrate was analyzed on the UV–vis spectrometer. Besides, the consecutive reactions were performed at the same conditions to investigate the stability of ZnFe2O4/TiO2. 3. Results and discussion XRD patterns of the pure ZnFe2O4, TiO2 and ZnFe2O4/TiO2 are shown in Fig. 1. For pure TiO2,the three strongest peaks at 2 values of 25.3∘, 38.6∘ and 48.1∘ clearly indicated that anatase TiO2 was prepared successfully [32]. The diffraction peaks of the ZnFe2O4/TiO2 at 2 values of 18.2∘, 29.9∘, 35.3∘, 42.8∘, 53.1∘, 56.6∘, 62.5∘, 70.5∘and 74.5∘ can be assigned to the reflection of (1 1 1), (2 2 0), (3 1 1), (4 0 0), (4 2 2), (5 1 1), (4 4 0), (6 2 0) and (6 2 2) planes of the cubic ZnFe2O4 with spinel structure, respectively (JCPDS Card no. 22- 1012) [33,34]. And the weak diffraction peaks at 2 values of 48.0∘ and 68.8∘ may be assigned to the reflection of (2 0 0) and (1 1 6) planes of anatase TiO2 (JCPDS Card no. 21-1217), respectively [32]. The solution combustion ignited at 623K may cause an uneven distribution of components in the reaction container, which results in the formation of a small amount of impurities, Fe2O3 and ZnO during the combustion process [35].
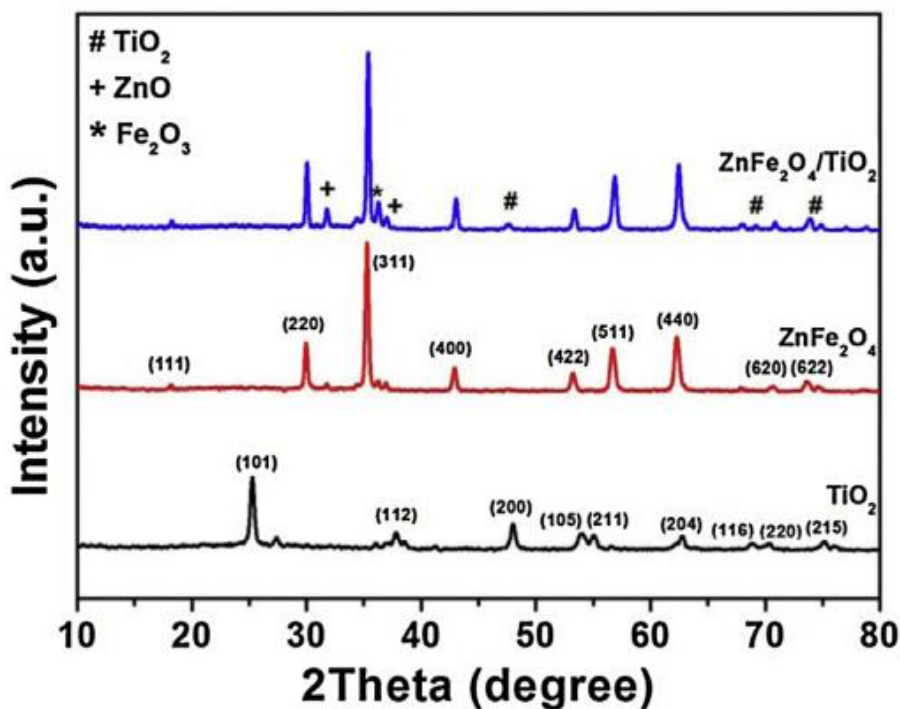
Fig. 1. XRD patterns of samples.

SEM images of ZnFe2O4/TiO2 with the different magnifications are shown in Fig. 2a and b. The anomalous sponge-like shape of ZnFe2O4/TiO2 with porous structure and rough surface were formed by the sustained release of gas (CO_2, N_2 and water vapor) during the combustion process, which is a remarkable characteristic of samples synthesized by solution combustion method [36,37]. The growth mechanism of ZnFe2O4 can be represented by the following equation: $9Zn(NO_3)_2 + 18Fe(NO_3)_3 + 40C_2H_5NO_2 = 9ZnFe_2O_4 + 100H_2O + 80CO_2 + 56N_2$ As depicted in Fig. 2c, N_2 adsorption/desorption isotherms of the ZnFe2O4/TiO2 corresponds to the IUPAC type II pattern with an H3 hysteresis loop, indicating the existence of mesoporous structure in synthesized sample. Noticeably, surface tridimensional structure of the mesoporous materials leads to the facile adsorption/desorption equilibrium and better mass transfer for the reactants and products, hence may improve the photocatalytic activity. Moreover, the abrupt increase in adsorption branch combined with the sharp decline in desorption branch is observed at the P/P0 value approximately greater than 0.9. This increase is generally due to the capillary condensation of N_2 into the mesoporous structure, indicating good homogeneity of these photocatalysts and fairly small pore sizes (the inset of Fig. 2c). Furthermore, TEM image in Fig. 2d showed that TiO2 nanoparticles were embedded tightly into the ZnFe2O4 framework, which can be attributed to strong reaction during the ignition process of solution combustion. The high resolution TEM image (Fig. 2e) further revealed the lattice fringes of 0.1667 nm and 0.1944 nm corresponding to the interplanar spacing of the (2 1 1) and (3 3 1) planes of TiO2 and ZnFe2O4, respectively. Notably, the EDS spectra (Fig. 2e) clearly indicated that the sample was composed of Zn, Fe, Ti and O elements. The Cu peaks came from the supporting copper grid. Based on these observations, it is suggested that the heterojunction structure was formed during the facile synthesis process.
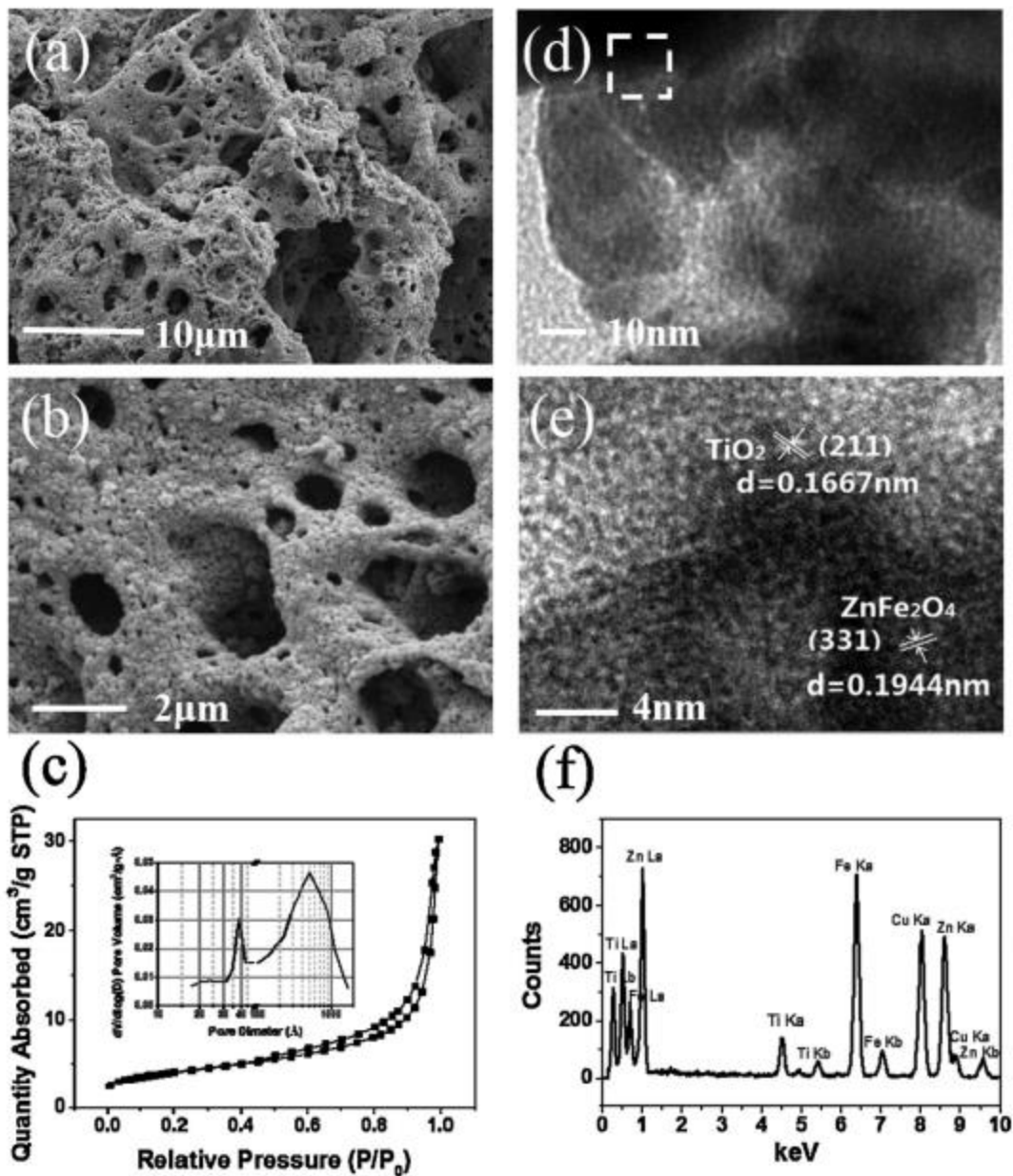
Fig. 2. The morphology and structure of ZnFe2O4/TiO2. (a and b) SEM images; (c) N2 adsorption/desorption isotherm and the inset is the pore size distributions; (d) TEM image; (e) HRTEM image of the square area in (d) and (f) EDS spectrum.

In order to determine the surface chemical composition and valence state of the ZnFe2O4/TiO2 samples overall, XPS spectra were collected in Fig. 3. Carbon was ascribed to the adventitious hydrocarbon from the XPS instrument itself. It shows that Zn, Fe, Ti and O elements coexisted in the composites. Fig. 3b–d displays the high-resolution XPS of Zn, Fe and Ti, respectively. The peaks at 1020.0 eV and 1043.2 eV are assigned to Zn 2p3/2 and 2p1/2, respectively. The peaks at 710.7 eV and 724.1 eV are attributed to 2p3/2 and 2p1/2 for

Fe3+ at octahedral sites, respectively. The satellite peaks at 719.5 eV and 733.6 eV confirm the oxidation state of iron is 3+. All these assignments are characteristics of Zn2+ and Fe3+ in ZnFe2O4 [33,38]. For Ti 2p region, it can be fitted into two peaks: Ti 2p1/2 and 2p3/2, which appear at 464.2 eV and 458.5 eV, respectively. These values agree with XPS data of Ti4+ in pure anatase TiO2 in literature [39]. The results indicate that Ti ions had not been incorporated in lattice with high temperature in short time during the ignition process of solution combustion, which is consistent with XRD results.
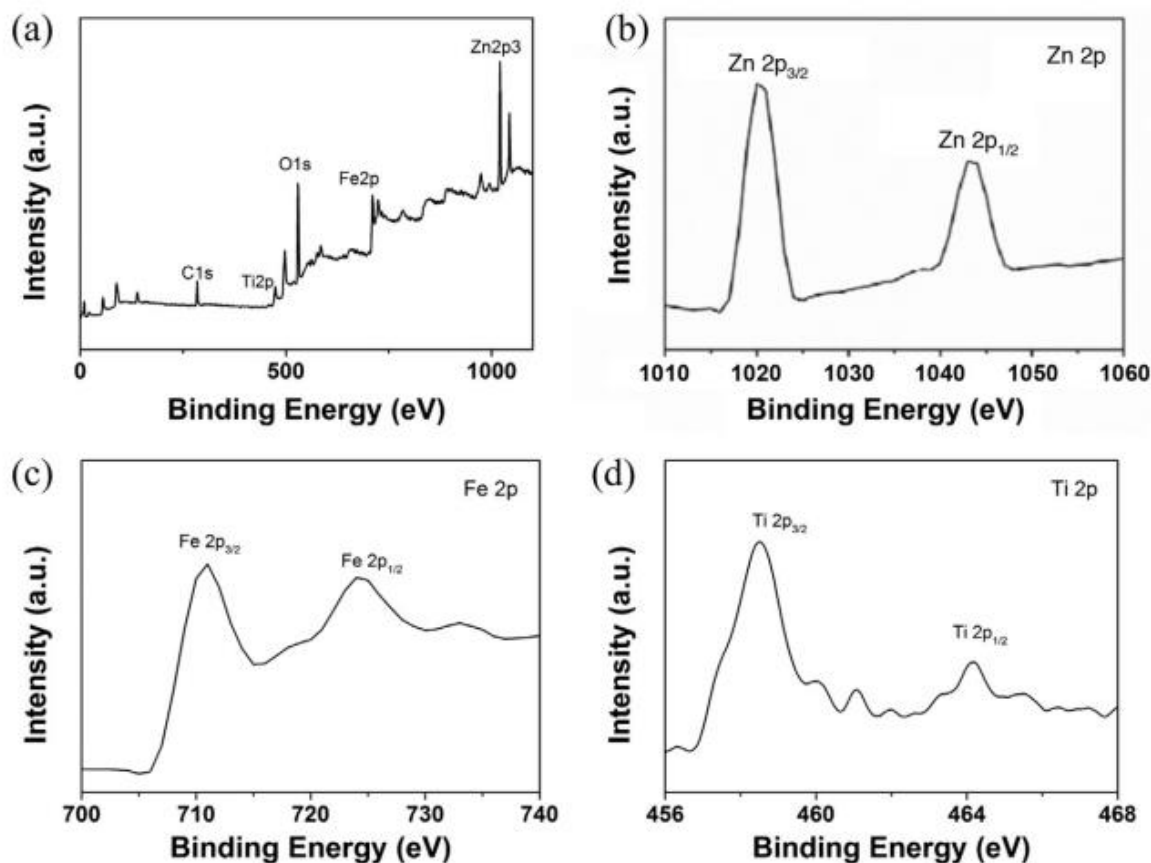

Fig. 3. XPS spectra of (a) full spectra scan; (b) Zn 2p; (c) Fe 2p and (d) Ti 2p.

To investigate the optical properties,the samples were analyzed by UV–vis DRS and the spectra were shown in Fig. 4. TiO2 mainly Fig. 4. UV–vis DRS of samples. responses to the ultraviolet light, while ZnFe2O4 and ZnFe2O4/TiO2 exhibit high absorption intensity in a wide region from 300 nm to 800 nm. The enhanced absorption in the visible light region of ZnFe2O4 can be attributed to photogenerated electron transition from O 2p orbital into Fe 3d orbital according to general definition of the energy band structures of ZnFe2O4 [36]. Meantime, ZnFe2O4/TiO2 shows a slight blue shift of the absorption threshold and higher absorption intensity than that of ZnFe2O4. It can be attributed to the formation of new level

between the VB and CB of ZnFe2O4 by coupling with TiO2 nanoparticles, which promotes the carriers mobility and further enhances the absorption. Besides, the porous morphology of the sponge-like ZnFe2O4/TiO2 appropriately functions as a good light harvesting system, which is also favorable to improve the absorption ability and subsequently results in the efficient utilization of visible light.
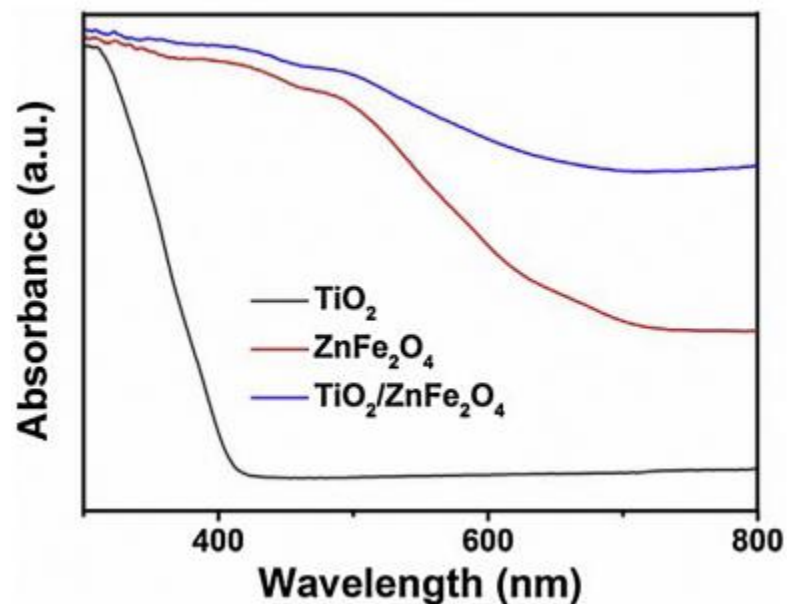

Fig. 4. UV–vis DRS of samples.

As known, PL spectrum is closely related to the recombination of excited electrons and holes, which can be utilized to reveal the electronic-transition-correlated energy levels. As depicted in Fig. 5, for the pure TiO2, no PL signal was detected because the excitation energy of 420 nm (2.85 eV) was lower than the bandgap of TiO2. However, this energy is high enough to excite electrons at VB of ZnFe2O4/TiO2 and ZnFe2O4 to the bottom of the CB where their mobility enables them to reach certain defect sites or elsewhere [40]. It was observed that the shapes of the PL spectra of ZnFe2O4/TiO2 and ZnFe2O4 are similar, indicating the dominant role of ZnFe2O4 in PL generation. The lower emission intensity of ZnFe2O4/TiO2 implies its lower recombination rate, which may be attributed to the formation of heterojunction between ZnFe2O4 and TiO2.
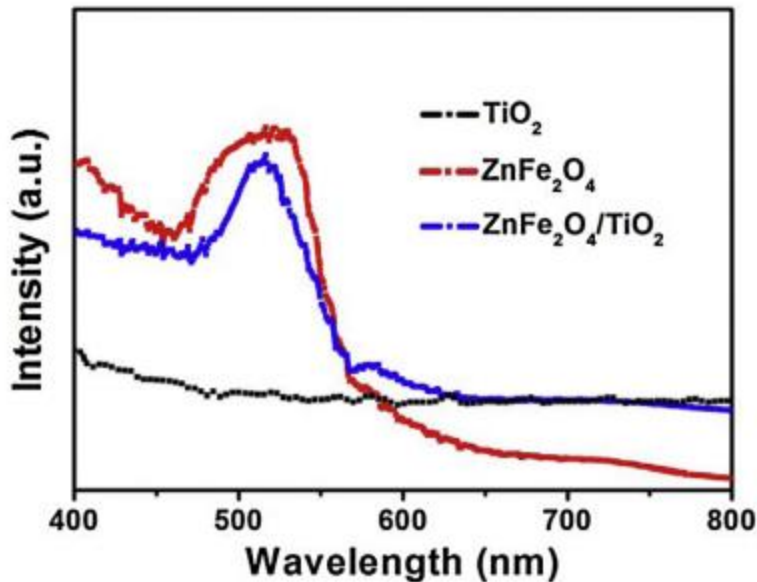
Fig. 5. The PL spectra of samples with the excitation wavelength of 420 nm.

The photocatalytic activities of the samples for MB degradation under visible light irradiation were shown in Fig. 6a. To distinguish the effect of adsorption, photolysis and photocatalysis on the MB degradation, some controlling experiments were carried out and the corresponding data are also presented. It was found that about 4.2% MB was adsorbed on ZnFe2O4/TiO2 after the adsorption–desorption equilibrium was reached during the adsorption experiment of ZnFe2O4/TiO2 in dark. The degradation of MB under visible light irradiation without the photocatalyst, namely self-photolysis, was also performed, and only about 4.5% of MB was converted in 2 h. Obviously, ZnFe2O4/TiO2 exhibited the highest photocatalytic activity with MB degradation rate of 93.2% under visible light irradiation. As shown in Fig. 6b, the main absorption peak at 664 nm corresponding to auxochromic groups of MB molecules decreased rapidly with extension of the irradiation time in the first hour. Further irradiation led to no absorption peak in the whole spectrum, which indicates the complete decomposition of MB in 2 h. The enhanced activity may depend on the synergistic effects as follows. Firstly, ZnFe2O4/TiO2 extended the spectral response to the visible light region as revealed by UV–vis DRS results. Meantime, the sponge-like morphology of ZnFe2O4/TiO2 functioned as a good light harvesting structure and thus enhanced absorption intensity of the irradiation light. Secondly, the specific morphology with surface tridimensional structure was favorable for the facile adsorption/desorption equilibrium and better mass transfer of the reactants and products. Lastly, as revealed by PL spectra, the recombination of photogenerated electron–hole pairs were effectively inhibited by the heterojunction structure and thus prolonged the lifetime of charge carriers of ZnFe2O4/TiO2. A stability test of ZnFe2O4/TiO2 was carried out and the result is presented in Fig. 6c. It can

be seen that the degradation rate of MB slightly decreased to 85.7% after five consecutive reaction runs, indicating a good photocatalytic stability of ZnFe2O4/TiO2. In addition, ZnFe2O4/TiO2 provided a convenient separation and recycling means of the photocatalyst in suspension system due to the magnetic property of ZnFe2O4 (Fig. 6d).
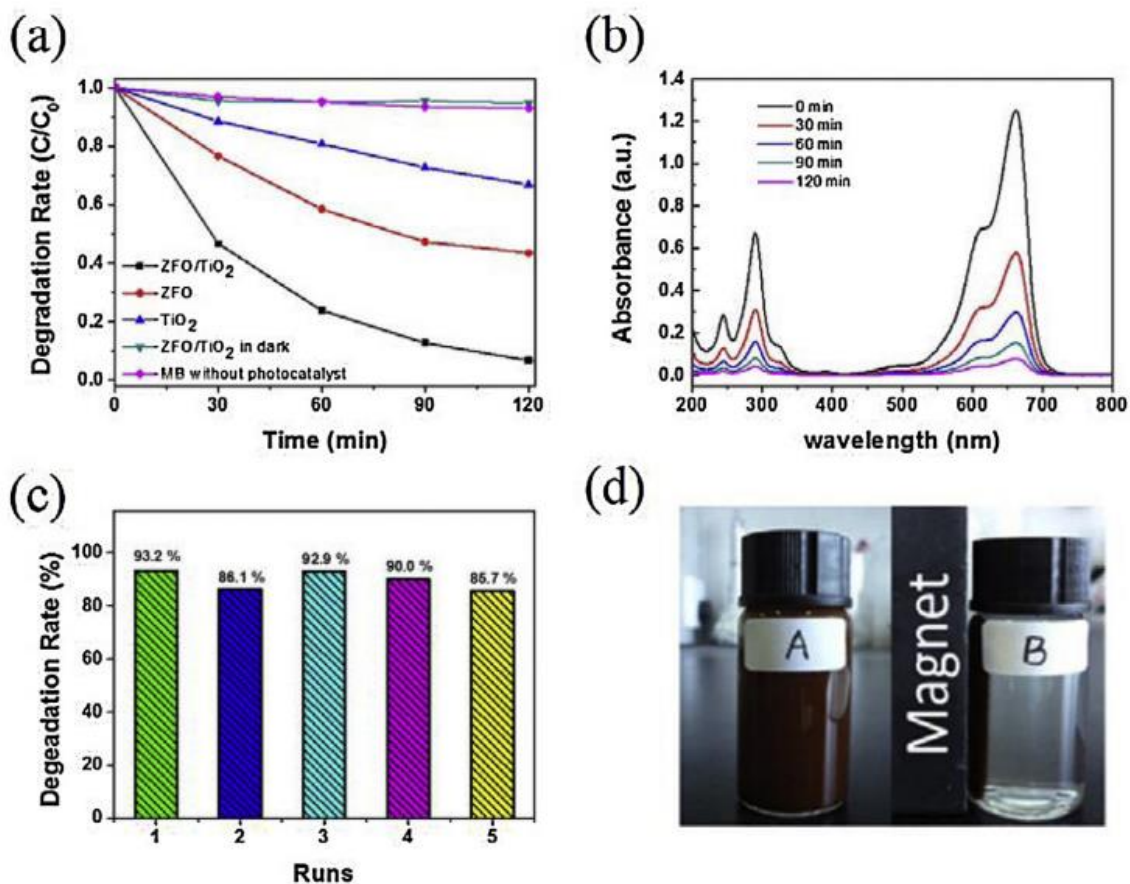

Fig. 6. (a) Photocatalytic activity of samples for the degradation of MB; (b) the temporal changes in the absorption spectra of MB over ZnFe2O4/TiO2; (c) photocatalytic activities of ZnFe2O4/TiO2 for five consecutive reaction runs and (d) images of the magnetism separation of ZnFe2O4/TiO2 suspension without (A) and with (B) a magnet.

Based on these, a photocatalytic mechanism of ZnFe2O4/TiO2 was proposed as illustrated in Fig. 7. As known, anatase TiO2 is normally an intrinsic p-type semiconductor disregarding the introduction of the impurity level, and ZnFe2O4 generally exhibits the characteristic properties of n-type semiconductor [40]. According to the energy band theory of semiconductor and the mobility characteristics of carriers at a heterojunction structure, an internal static electric field (Einter) can be established in the space charge region at the interface between ZnFe2O4 and TiO2 for the equivalence of the Fermi levels with the electric field direction from ZnFe2O4 to TiO2. As a consequence, the energy bands at the junction

section will bend. Fig. 7a illustrated the change of band structure without considering the effect of interface state. In the presence of visible light radiation, ZnFe2O4 can be excited, resulting in the generation of electrons in CB and the holes in VB of ZnFe2O4 [22,34]. While, TiO2 with a bandgap of 3.2 eV cannot be excited in this case [2,6]. Since the electric field at the interface facilitates the migration of electrons from the VB of p-type semiconductor to the VB of n-type semiconductor [40],the electrons in VB of TiO2 could easily transfer to the VB of ZnFe2O4, alongside the generation of holes in the VB of TiO2. The holes in the VB of TiO2 could initiate photocatalytic oxidation reactions. As shown in Fig. 7b, they may directly react with contaminations (Eq.(1)) or interact withsurface-boundH2O or OH− to form hydroxyl radicals (•OH) which are extremely strong oxidant for the mineralization of most organic contaminations (Eq. (2)) [3]. Noticeably,the excited electrons in ZnFe2O4 canalso create a simultaneous reduction, reacting with the adsorbed molecular oxygen to yield O2 •− (Eq. (3)). The generated O2 •− may further combine with H+ to produce •OH [22]. To confirm the existence of active •OH in the process of photocatalytic degradation, ESR spectra was investigated in the same condition and shown in Fig. 8. The appearance of characteristic 1:2:2:1 quartet signal indicated that •OH were generated during the photocatalytic reaction on ZnFe2O4/TiO2. The signal intensity showed an increase with the time lapsing in the first minutes of the photocatalytic reaction, revealing that more and more hydroxyl radicals were produced and hence MB could be degraded gradually by these radicals. The steady signal was observed after irradiation for 120 s, indicating a steady generation rate of •OH by ZnFe2O4/TiO2. Most importantly, the internal field created by a heterojunction between TiO2 and ZnFe2O4 promotes the separation of photogenerated charge carriers. The probability of e−–h+ recombination was effectively suppressed and the lifetime of the charge carriers was lengthened, which improved the photocatalytic activity.
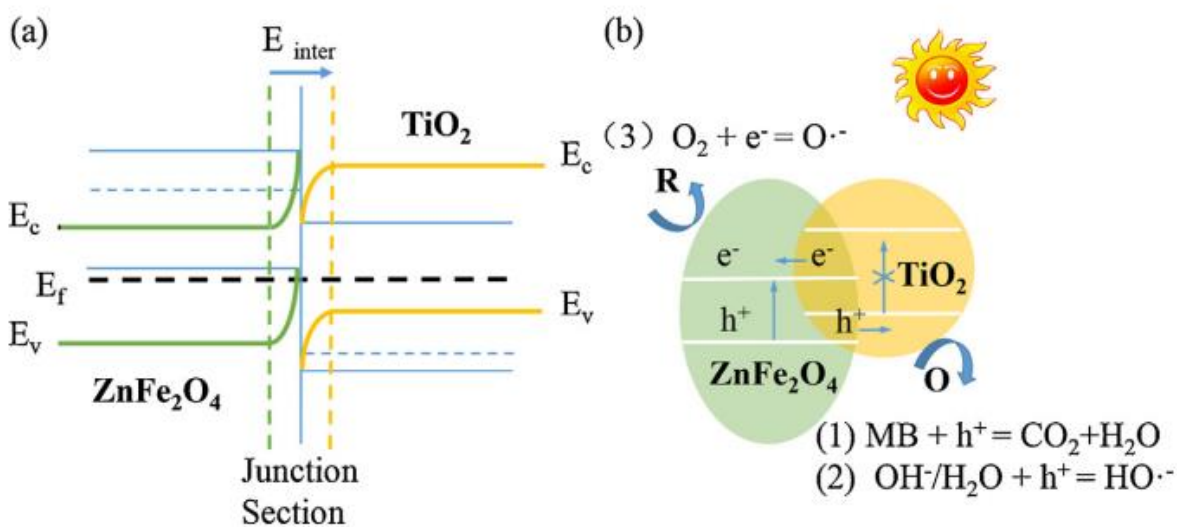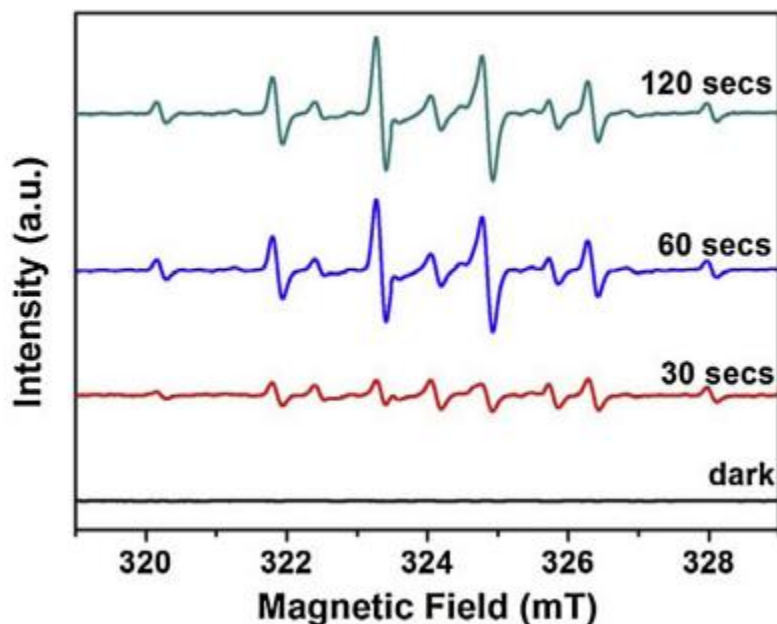
Fig. 7. Schematics of (a) the formation of ZnFe2O4/TiO2 heterojunction and (b) the photocatalytic degradation mechanism of MB on ZnFe2O4/TiO2.

Fig. 8. DMPO spin-trapping ESR spectra for the DMPO-•OH in aqueous dispersion of ZnFe2O4/TiO2 with visible light irradiation.

4. Conclusions

ZnFe2O4/TiO2 photocatalyst was facilely synthesized by a solution combustion method. ZnFe2O4/TiO2 shows enhanced photocatalytic activity of MB degradation with a degradation rate of 93.2% in 2 h under visible light irradiation and exhibits an excellent stability. The high activity of ZnFe2O4/TiO2 can be attributed to the sponge-like porous morphology and heterojunction structure of the composite, which promotes the adsorption of reaction species and absorption intensity of irradiation light, and improves the photogenerated electron–hole pairs' separation and interfacial charge transfer. The photocatalytic mechanism of MB degradation is proposed with the definition of the internal static electric field in the space charge region at the interface of semiconductors. This work might provide a relatively simple synthesis pathway for fabricating heterojunction photocatalysts. The synthesized sponge-like ZnFe2O4/TiO2 with the characteristic of magnetic recycling would be a promising photocatalyst for wastewater remediation.

References

[1] A. Fujishima, K. Honda, Electrochemical photolysis of water at a semiconductor electrode, Nature 238 (1972) 37–38. [2] R. Asahi, T. Morikawa, T. Ohwaki, K. Aoki, Y. Taga, Visible light photocatalysis in nitrogen-doped titanium oxides, Science 293 (2001) 269–271. [3] M.R. Hoffmann, S.T. Martin, W. Choi, D.W. Bahnemann, Environmental applications of semiconductor photocatalysis, Chem. Rev. 95 (1995) 69–96. [4] K. Nakata, A. Fujishima, TiO2 photocatalysis: design and applications, J. Photochem. Photobiol. C 13 (2012) 169–189. [5] M. Pelaez, N.T. Nolan, S.C. Pillai, M.K. Seery, P. Falaras, A.G. Kontos, P.S.M. Dunlop, J.W.J. Hamilton, J.A. Byrne, K. O'Shea, M.H. Entezari, D.D. Dionysiou, A review on the visible light active titanium dioxide photocatalysts for environmental applications, Appl. Catal. B: Environ. 125 (2012) 331–349. [6] J.G. Yu, Q.J. Xiang, M.H. Zhou, Preparation, characterization and visible-lightdriven photocatalytic activity of Fe-doped titania nanorods and first-principles study for electronic structures, Appl. Catal. B: Environ. 90 (2009) 595–602. [7] X.L. Zhang, R. Qiao, J.C. Kim, Y.S. Kang, Inorganic cluster synthesis and characterization of transition-metal-doped ZnO hollow spheres, Cryst. Growth Des. 8 (2008) 2609–2613. [8] X.B. Cao, L. Gu, X.M. Lan, C. Zhao, D. Yao, W.J. Sheng, Spinel ZnFe2O4 nanoplates embedded with Ag clusters: preparation, characterization, and photocatalytic application, Mater. Chem. Phys. 106 (2007) 175–180. [9] L.J. Liu, G.L. Zhang, L. Wang, T. Huang, L. Qin, Highly active S-modified ZnFe2O4 heterogeneous catalyst and its photo-Fenton behavior under UV–visible irradiation, Ind. Eng. Chem. Res. 50 (2011) 7219–7227.

[10] R. Asahi, T. Morikawa, T. Ohwaki, K. Aoki, Y. Taga, Visible-light photocatalysis in nitrogen-doped titanium oxides, Science 293 (2001) 269–271. [11] M.H. Zhou, J.G. Yu, Preparation and enhanced daylight-induced photocatalytic activity of C,N,S-tridoped titanium dioxide powders, J. Hazard. Mater. 152 (2008) 1229–1236. [12] G.P. Dai, S.Q. Liu, Y. Liang, H.J. Liu, Z.C. Zhong, A simple preparation of carbon and nitrogen co-doped nanoscaled TiO2 with exposed (0 0 1)facetfor enhanced visible-light photocatalytic activity, J. Mol. Catal. A: Chem. 368 (2013) 38–42.

[13] L.F. Qi, J.G. Yu, M. Jaroniec, Preparation and enhanced visible-light photocatalytic H2-production activity of CdS-sensitized Pt/TiO2 nanosheets with exposed (0 0 1) facets, Phys. Chem. Chem. Phys. 13 (2011) 8915–8923. [14] R. Abe, K. Shinmei, N. Koumura, K. Hara, B. Ohtani, Visible-light-induced water splitting based on two-step photoexcitation between dye-sensitized layered niobate and tungsten oxide photocatalysts in the presence of a triiodide/iodide shuttle redox mediator, J. Am. Chem. Soc. 135 (2013) 16872–16884. [15] L.Kong, Z.Jiang, T.Xiao, L. Lu,M.O.Jones, P.P. Edwards, Exceptional visible-lightdriven photocatalytic activity over BiOBr–ZnFe2O4 heterojunctions, Chem. Commun. 47 (2011)

5512–5514. [16] Z.H. Yuan, L.D. Zhang, Synthesis, characterization and photocatalytic activity of ZnFe2O4/TiO2 nanocomposite, J. Mater. Chem. 11 (2001) 1265–1268.

[17] K.Z. Lv, J. Li, X.X. Qing, W.Z. Li, Q.Y. Chen, Synthesis and photo-degradation application of WO3/TiO2 hollow spheres, J. Hazard. Mater. 189 (2011) 329–335. [18] H.Q. Jiang, M. Nagai, K. Kobayashi, Enhanced photocatalytic activity for degradation of methylene blue over V2O5/BiVO4 composite, J. Alloys Compd. 479 (2009) 821–827. [19] C.H. Kim, Y. Myung, Y.J. Cho, H.S. Kim, S.H. Park, J. Park, J.Y. Kim, B. Kim, Morphology-tuned synthesis of single-crystalline V5Si3 nanotubes and nanowires, J. Phys. Chem. C 113 (2009) 7085–7090. [20] S. Xuan, F. Wang, J.M.Y. Lai, K.W.Y. Sham, Y.X.J. Wang, S.F. Lee, J.C. Yu, C.H.K. Cheng, K.C.F. Leung, Synthesis of biocompatible mesoporous Fe3O4 nano/microspheres with large surface area for magnetic resonance imaging and therapeutic applications, ACS Appl. Mater. Interfaces 3 (2011) 237–244. [21] J. Yin, L.J. Bie, Z.H. Yuan, Photoelectrochemical property of ZnFe2O4/TiO2 double-layered films, Mater. Res. Bull. 42 (2007) 1402–1406. [22] M.Y. Wang, L. Sun, J.H. Cai, P. Huang, Y.F. Su, C.J. Lin, A facile hydrothermal deposition of ZnFe2O4 nanoparticles on TiO2 nanotube arrays for enhanced visible light photocatalytic activity, J. Mater. Chem. A 1 (2013) 12082–12087. [23] X.Y. Li, Y. Hou, Q.D. Zhao, G.H. Chen, Synthesis and photoinduced chargetransfer properties of a ZnFe2O4-sensitized TiO2 nanotube array electrode, Langmuir 27 (2011) 3113–3120.

[24] Y. Hou, X.Y. Li, Q.D. Zhao, X. Quan, G.H. Chen, Electrochemical method for synthesis of a ZnFe2O4/TiO2 composite nanotube array modified electrode with enhanced photoelectrochemical activity, Adv. Funct. Mater. 20 (2010) 2165–2174. [25] S.F. Chen, H.Y. Zhang, X.L. Yu, W. Liu, J.E. Wang, Q.C. Liu, L. Chen, Preparation, characterization and activity evaluation of heterojunction ZrTi2O6/TiO2 photocatalyst, Mater. Chem. Phys. 124 (2010) 1057–1064. [26] Y.G. Chen, S.W. Liu, H.P. Zhang, Z.L. Xiu, X.J. Yu, E.H. Wang, T.G. Li, Preparation and photocatalytic property of Sr(Zr1−xYx)O3/TiO2/CdS heterojunction photocatalysts, Mater. Sci. Eng. B 174 (2010) 187–190. [27] S.Y. Chai, Y.J. Kim, M.H. Jung, A.K. Chakraborty, D. Jung, W.I. Lee, Heterojunctioned BiOCl/Bi2O3: a new visible light photocatalyst, J. Catal. 262 (2009) 144–149. [28] Z.B. Wu, F. Dong, Y. Liu, Enhancement of the visible light photocatalytic performance of C-doped TiO2 by loading with V2O5, Catal. Commun. 11 (2009) 82–86. [29] L.F. Cui, M.T. Niu, G.X. Chen, Fabrication and structure characterization of MnCO3/-Fe2O3 nanocrystal heterostructures, Mater. Lett. 63 (2009) 2499–2502. [30] R. Brahimi, Y. Bessekhouad, A. Bouguelia, M. Trari, CuAlO2/TiO2 heterojunction applied to visible light H2 production, J. Photochem. Photobiol. A 186 (2007) 242–247. [31] B. Liu, H.C. Zeng, Carbon nanotubes supported mesoporous mesocrystals of anatase TiO2, Chem. Mater. 20 (2008) 2711–2718. [32] M. Ba-Abbad, A.H. Kadhum, A. Mohamad, M.S. Takriff, K. Sopian, Synthesis and catalytic activity of TiO2 nanoparticles for photochemical oxidation of concentrated chlorophenols under direct solar radiation, Int. J.

Electrochem. Sci. 7 (2012) 4871–4888. [33] W.N. Fu, Y.H. Wang, C. He, J.L. Zhao, Photocatalytic degradation of acephate on ZnFe2O4–TiO2 photocatalyst under visible-light irradiation, J. Adv. Oxid. Technol. 15 (2012) 177–182. [34] H. Lv, L. Ma, P. Zeng, D. Ke, T. Peng, Synthesis of floriated ZnFe2O4 with porous nanorod structures and its photocatalytic hydrogen production under visible light, J. Mater. Chem. 20 (2010) 3665–3672. [35] M.A. Valenzuela, P. Bosch, J. Jimenez-Becerrill, O. Quiroz, A.I. Paez, Preparation, characterization and photocatalytic activity of ZnO, Fe2O3 and ZnFe2O4, J. Photochem. Photobiol. C 148 (2002) 177–182. [36] S. Sun, X.Y. Yang, Y. Zhang, F. Zhang, J.J. Ding, J. Bao, C. Gao, Enhanced photocatalytic activity of sponge-like ZnFe2O4 synthesized by solution combustion method, Prog. Nat. Sci. 6 (2012) 639–643. [37] J.J. Moore, H.J. Feng, Combustion synthesis of advanced materials: Part 2—Reaction parameters, Prog. Mater. Sci. 39 (1995) 275–316. [38] H. Xue, Z.H. Li, X.X. Wang, X.Z. Fu, Facile synthesis of nanocrystalline zinc ferrite via a self-propagating combustion method, Mater. Lett. 61 (2007) 347–350.

[39] G. Mishra, K.M. Parida, S.K. Singh, Solar light driven Rhodamine B degradation over highly active -SiC–TiO2 nanocomposite, RSC Adv. 4 (2014) 12918–12928.

[40] R. Marschall, Semiconductor composites: strategies for enhancing charge carrier separation to improve photocatalytic activity, Adv. Funct. Mater. 24 (2014) 2421–2440.